ECS Transactions, 69 (1) 113-123 (2015)
10.1149/06901.0113ecst ©The Electrochemical Society

Challenges with Quantum Chemistry-Based Screening of Electrochemical Stability of Lithium Battery Electrolytes

Oleg Borodin,[a] Marco Olguin[a] Carrie E. Spear,[b] Kenneth W. Leiter,[b] Jaroslaw Knap[b], Gleb Yushin,[c] Adam S. Childs,[b] Kang Xu,[a]

[a] Electro-Chemistry Branch, RDRL-SED-C, Powder Mill Rd. 2800, US Army Research Laboratory, Adelphi, MD, 20783-1138, USA

[b] Simulation Sciences Branch, RDRL-CIH-C, US Army Research Laboratory, Aberdeen Proving Ground, MD, 21005-5066, USA

[c] School of Materials Science and Engineering, Georgia Institute of Technology, Atlanta, GA 30332

Challenges with the quantum chemistry based-screening of electrochemical stability of solvents and salts with potential applications in lithium batteries are discussed. Initial high throughput screening of carbonate and phosphate-based electrolyte solvents provided insight into first and second reduction and oxidation potentials and reorganization energies of these solvents. It has been found that it was important to include a lithium cation in the screening of semifluorinated solvents. Two reduction pathways have been found for lithium complexed with semifluorinated solvents and salts such as lithium bis(fluorosulfonyl)imide (LiFSI): the low rate defluorination reaction occurring at high potentials and fast solvent or anion reduction occurring at significantly lower potentials. A spontaneous deprotonation of carbonate solvents at the surface of the completely de-lithiated $LiNi_{0.5}Mn_{1.5}O_4$ cathode has been found.

Introduction

Development of novel electrolyte – electrode couples requires knowledge of key electrolyte electrochemical properties such as conductivity, transference number, melting points, flammability, vapor pressure, wettability of separator and electrolyte electrochemical stability window. Electrolytes should be either electrochemically stable at the operating voltage of electrodes or if they reduce or oxidized at the negative or positive electrode, they should form a stable passivation layer as a result of redox reactions, decomposition and precipitation on electrode surfaces. Commonly used carbonate-based solvents typically undergo reduction at the graphite anodes forming a solid electrolyte interphase (SEI).(1-4) If a coherent SEI is not formed, continual electrolyte degradation and/or graphite exfoliation occurs. Because state of the art electrolytes are often multicomponent mixtures, it is important to know not only if each solvent or salt reduces at the electrode but also the order of the reduction stability for each electrolyte component. Knowledge of the preferential, or sacrificial, reduction is expected to provide a better control of the SEI composition and its properties.(5) Intriguingly, in addition to electrolyte reduction at anodes, certain electrolytes may undergo both reduction and oxidation at the cathode during battery cycling forming the passivation layer that could dramatically slow down cathode dissolution and capacity

fade.(6) Ability to control electrochemical stability is also important for rational design of redox shuttle additives that assist in overcharge protection(7-9), or reduce overpotential during the first charge and lead to in-situ formation of the passivation layer.(10)

Previous quantum chemistry (QC) calculations were used to examine the oxidative stability of solvents,(11-19) redox-shuttles,(8, 9, 20) anions(21-24), and solvent decomposition pathways.(15, 25, 26) Invaluable insight into interfacial reduction reactions at the anode and cathode was provided from ab initio MD simulations(26-33) Initial high-throughput reports of electrolyte electrochemical properties focused on screening of the HOMO-LUMO gaps, electrochemical stability of isolated molecules and development of the workflow infrastructure.(34-36) Current work will provide further insight into electrolyte reduction and oxidation stability from QC calculations. In this work, we apply a recently developed distributed multi-scale computing framework(37) to the initial screening of electrochemical stability and initial decomposition reactions for carbonate and sulfone-based solvents and discuss the first and second adiabatic oxidation and reduction stability and reorganization energy for these compounds. Furthermore, we discuss the need for further improvement of the screening methodology that would require adding the lithium cation, multiple solvents or electrode surfaces.

High Throughput Screening of Isolated Solvents

The initial screening of 100 carbonate molecules and 300 phosphate molecules was performed using the distributed multi-scale computing framework developed by Knap et al.(37). The framework employs the concept of distributed multi-scale computing to create a hierarchy of at-scale models that spans across geographically scattered computational resources. The multi-scale hierarchy originates with a high-throughput analysis algorithm executing on a computer system, such as a workstation. The algorithm utilizes a Distributor module to route requests for the evaluation of required at-scale models to a remote computer system with available computational resources (e.g. processors, co-processors or graphic processors). We note here that the remote computer system can be a large high-performance system or a smaller system, such as a workstation. An additional module executing on a remote system manages the evaluation of at-scale models. More specifically, it carries out the following tasks: 1) collects sub-model evaluation requests from Distributor; 2) schedules the evaluation of these requests on available resources; and 3) communicates the results of the sub-model evaluation requests back to Distributor. We emphasize that the handling of at-scale model evaluations is fully asynchronous, i.e. there is no explicit synchronization between the execution of the high-throughput algorithm and any of the at-scale models. A detailed description of the high-throughput framework is available elsewhere.(37)

The absolute oxidation and reduction potentials of a complex M relative to an electron at rest in vacuum, ($E^0_{abs}(M)$), is given by Eq. 1 and 2, respectively,

$$E^0_{oxidation}(M) = [\Delta G_e + \Delta G^0_S(M^+) - \Delta G^0_S(M)]/F, \quad (1)$$

$$E^0_{reduction}(M) = -[\Delta G_e + \Delta G^0_S(M^-) - \Delta G^0_S(M)]/F, \quad (2)$$

where ΔG_e is the ionization free energy or electron affinity in gas-phase at 298.15 K; $\Delta G_S(M^+)$, $\Delta G_S(M^-)$ and $\Delta G_S(M)$ are the free energies of solvation of the oxidized,

reduced and initial complexes, respectively; and F is the Faraday constant. We will also refer to oxidation potentials as free energies of the oxidation and reduction reactions and will distinguish them from the energies of the oxidation and reduction reactions that are calculated at 0 K and did not include entropic or zero-point corrections. The predicted values from QC calculations of the absolute $E_{abs}(M)$ are converted to the commonly used Li/Li^+ potential scale by subtracting 1.4 V in order to compare them with experimental data.(38) Solvent variation is expected to change this factor by 0.1-0.3 V because the variation of the lithium free energy of solvation in water, methanol, acetonitrile, hydrazine, and ammonia was reported to be in this range.(39) IUPAC recommends a SHE value of 4.42–4.44 V in the absolute potential scale at room temperature leading to the conversion factor used in this work.(40)

Details of the QC calculations and generation of the initial structures for screening were described elsewhere.(41) A brief summary is provided here. Gaussian g09 software was used for all calculations.(42) Initial structures were sourced from the PubChem database. Only neutral complexes were included in the screening set. Structures containing Cl, Na, K, Ca, Br, I, and Ba were discarded. Only small molecules containing less than 17 heavy atoms were chosen as large solvents tend to result in high electrolyte viscosity and low ionic conductivity. The M05-2X density functional was used because this functional and M06-2X were shown to accurately describe electron affinity (EA) and ionization potential (IP). M06-2X described the ionization potential (IP) potential better than M05-2X, while M05-2X yields a better description of electron affinity (EA).(43) The SMD implicit solvation model using acetone parameters was used because acetone dielectric constant ε=20.493 is similar to the value of the dielectric constant found in a typical mixture of linear and cyclic carbonates that are currently used in batteries. (44)

HOMO and LUMO energies are commonly used during high throughput screening of electrolytes as computationally inexpensive descriptors for the oxidation and reduction stability of electrolytes. The correlation between HOMO and oxidation stability is shown in Figure 1. While a good correlation is observed between HOMO energies and vertical oxidation stability (see Figure 1a), a noticeably worse correlation is observed between the HOMO energy and the adiabatic oxidation stability shown in Figure 1b with deviations from a linear fit larger than 1 eV observed for a number of compounds. Similarly, the LUMO energy correlates well with the vertical reduction stability as shown in Figure 2a. The correlation is better for higher reduction potentials and becomes worse for the lowest reduction potentials. Somewhat surprisingly, a very significant deviation between LUMO and adiabatic reduction potentials has been observed in Figure 2b. Manual examination of the worst outliers indicated that they either underwent a significant deformation or bond breaking occurred after the solvent accepted an electron. We suggest that the LUMO energy can be used only at the earliest stages of screening in order to obtain a lower bound for the reduction stability and more expansive adiabatic reduction potential calculations need to be performed for more reliable screening. DFT calculations also indicated that the majority of tested compounds were found to have a higher second reduction potential than the first reduction potential.(41) Thus, if the singly reduced species stick near the negative electrode long enough they are likely to undergo the second reduction reaction before their decomposition. (41) Analogously, a significant number of solvents had a second oxidation potential lower than the first oxidation potential, suggesting that two subsequent oxidations are likely to occur for a significant number of solvents if the radical does not desorb from the cathode surface fast enough. (41)

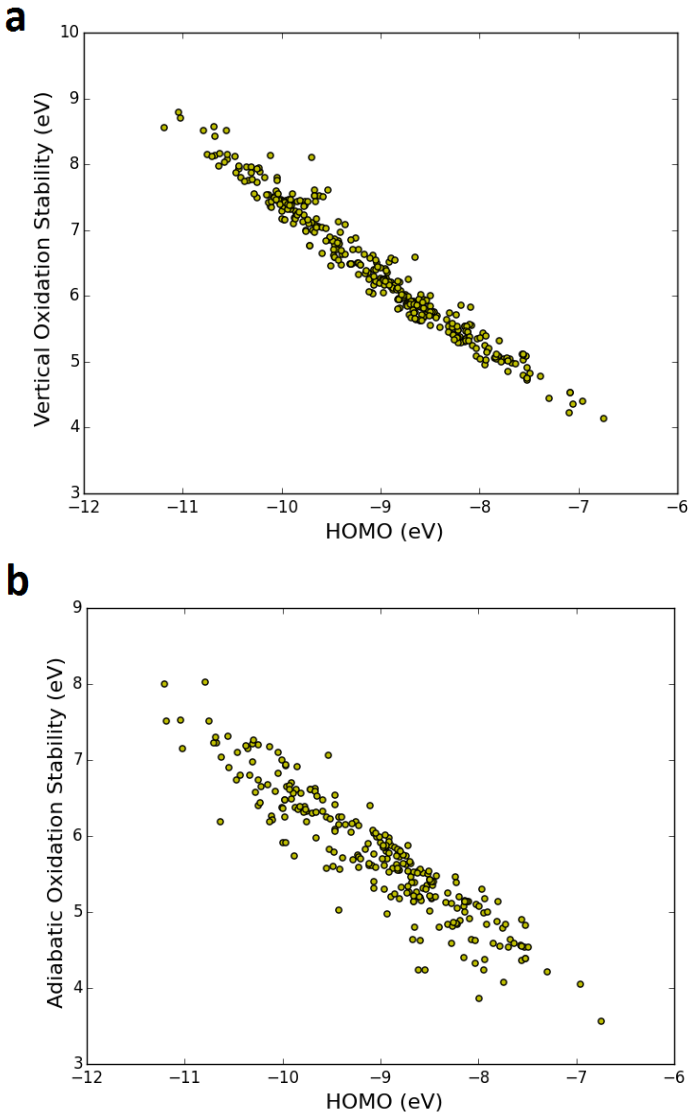

Figure 1. HOMO energies and vertical (a) and adiabatic (b) oxidation stability for the screened solvents from M05-2X/6-31+G(d,p) DFT calculations using SMD(ε=20) solvation model.

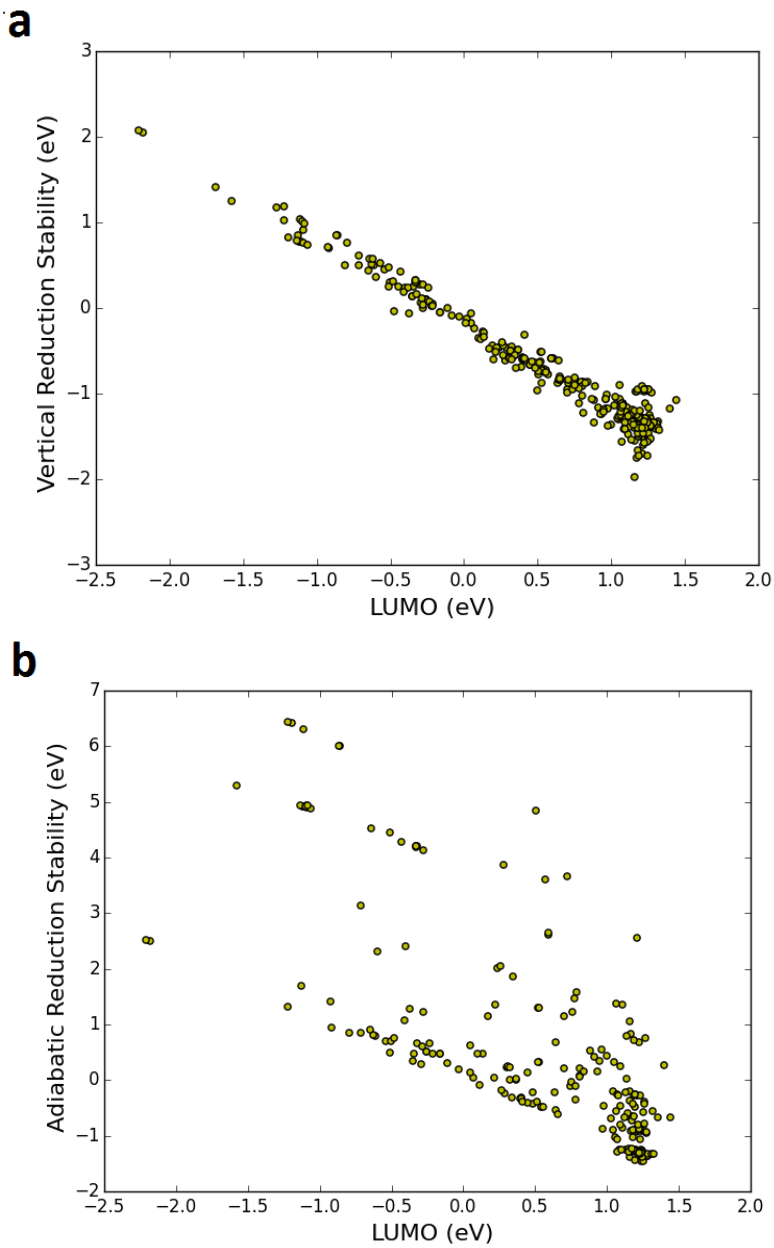

Figure 2. LUMO energies and vertical (a) and adiabatic (b) reduction stability of the screened solvents from M05-2X/6-31+G(d,p) DFT calculations using SMD(ε=20) solvation model.

Reduction Stability of Semifluorinated Electrolytes

While the screening of isolated solvents provides initial information on intrinsic stability of solvents it does not take into account possible intermolecular reactions that might proceed with a negligible, or in some cases substantial, barrier during electrolyte reduction or oxidation. For example, H-transfer reactions often occur during solvent oxidation.(38, 45-50) At the anode side, the solvent – lithium cation interaction polarize solvent and increase its reduction potential. However, interaction between the fluorinated group of the semifluorinated solvents and a lithium cation during reduction might have an additional significant impact on the reduction stability and decomposition reactions of

these electrolytes beyond the solvent polarization by Li^+. In order to illustrate the latter point, let's consider the calculated reduction potentials of EC/Li^+ and fluoroethylene carbonate (FEC) complexed with Li^+ as shown in Figure 3. Because there are multiple configurations of the reduced EC/Li^+ complexes, a variety of initial configurations need to be examined during screening.(41) Two of the most stable configurations of the reduced EC/Li are shown in Figure 3(b-c) suggesting reduction of the EC/Li^+ around 0.6 V vs. Li/Li^+. Fluorination of EC (creating FEC) increases its reduction potential up to 0.9 V vs. Li/Li^+ as shown in Figure 3f, which is slightly higher than the value of 0.75 V obtained from MP2/6-311++G(3df,2pd) calculations by Leung(30) in a similar implicit solvent but is in good agreement with the experimental value of 0.95 V vs. Li/Li^+.(51) When one considers the defluorination reaction coupled with FEC/Li^+ reduction (see Figure 3g) the predicted reduction potential is much higher ~1.7-2.3 V vs. Li/Li^+. Such reaction is expected to have a significant barrier as the Li^+ cation binding to fluorine of FEC is significantly less probable than binding to the carbonyl oxygen due to the higher energy of the FEC/Li^+ complex (e) compared to complex (d) by 0.3 eV. Nevertheless, the LiF formation is expected to occur first during the SEI formation cycle. This defluorination reaction is in accord with the experimental finding that addition of FEC resulted in a more pronounced peak around 1.7 V in the measured differential capacity for electrolytes with FEC additive.(52)

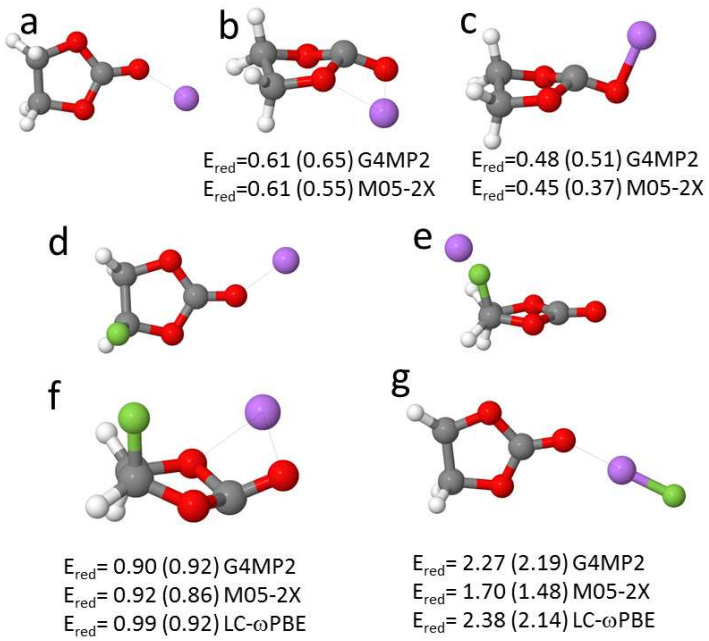

Figure 3. Optimized geometries from M05-2X/6-31+G** calculations with SMD(ε=20) of EC/Li^+ (a-c) and FEC/Li^+ (d-g). Complexes (a,d,e) have charge +1e, while reduced complexes (b-c, f-g) have total charge zero.

Such defluorination reactions coupled with the reduction of semifluorinated solvents complexed by Li^+ are not limited to FEC. Figure 4 and 5 demonstrate that the semifluorinated ethylmethyl carbonate and sulfolate (fluorotetraethyl sulfone FTMS) complexes with Li^+ also undergo defluorination around 2 V vs. Li/Li^+, while solvent reduction not coupled with LiF formation occurs at significantly lower potentials. Figures 4-5 also highlight a need to screen numerous configurations of the reduced clusters in

order to find the lowest energy. Defluorination reactions are not limited to solvents. Reduction of lithium bis(fluorosulfonyl)imide (LiFSI) aggregates and contract ion pairs was predicted to occur around 1.6-2.4 V vs. Li/Li^+ yielding LiF in good agreement with the experimentally observed values.(6)

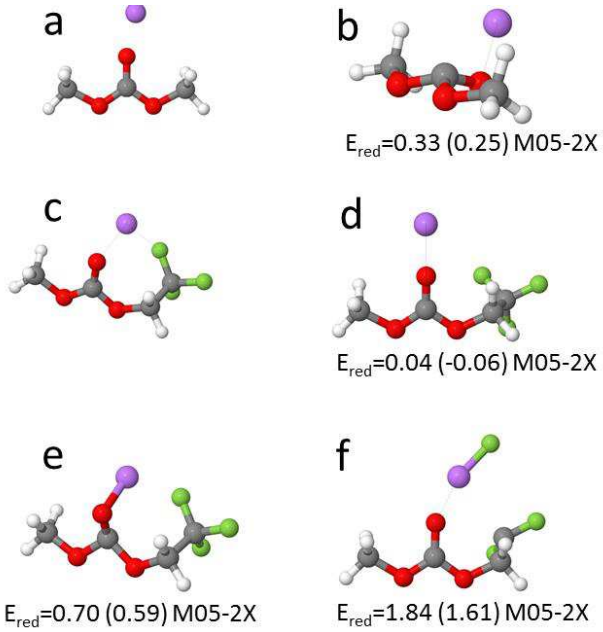

Figure 4. Optimized geometries from M05-2X/6-31+G** calculations with SMD(ε=20) of DMC/Li^+ (a-c) and DMC(CF_3)/Li^+ (d-g). Complexes (a,c) have charge +1e, while reduced complexes (b, d-f) have total charge zero.

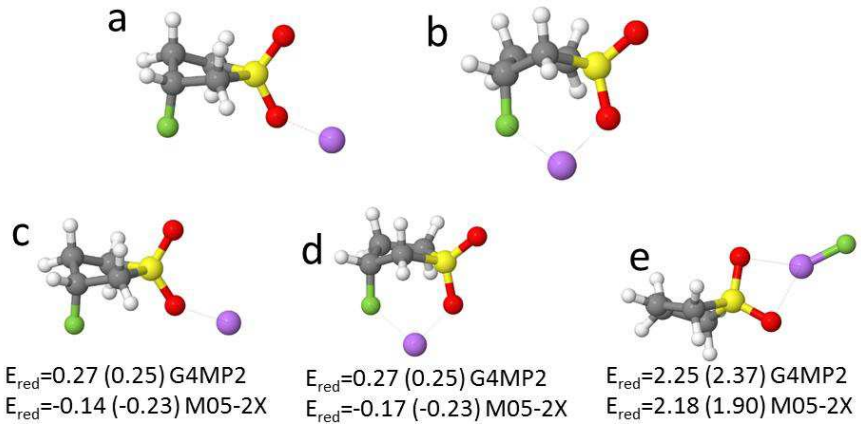

Figure 5. Optimized geometries from M05-2X/6-31+G** calculations with SMD(ε=20) of FTMS/Li^+ (a-c). Complexes (a,b) have charge +1e, while reduced complexes (c-e) have total charge zero.

Solvent Oxidation at Cathode Surface

In order to investigate the electrolyte/cathode interactions, DFT calculations were performed for single-molecule/cathode-surface configurations to examine the interaction of EC and DMC with the mixed valence high-voltage $LiNi_{0.5}Mn_{1.5}O_4$ (LNMO) transition metal oxide cathode material.(41) In this initial study, our focus was on the completely de-lithiated LMNO cathode in order to explore reactions at the extreme high state-of-charge potential where the spontaneous decomposition (i.e. negligible reaction barrier) of electrolytes is most likely to occur. The periodic plane-wave DFT+U calculations for the electrolyte/cathode interfaces were performed using the Vienna ab initio Simulation Package (VASP) with the spin-polarized Perdew-Burke-Ernzerhof exchange-correlation functional and the projector-augmented wave (PAW) scheme to treat core electrons.(53-57) Calculation details are described elsewhere.(41)

Structural relaxations were performed for systems consisting of the EC and DMC molecule adsorbed on the lowest surface energy [100] and [111] facets of the completely de-lithiated $Ni_{0.5}Mn_{1.5}O_4$ (NMO) spinel. One of the distinguishing structural features among the various electrolyte/cathode interface configurations studied is the number of hydrogen atoms from the solvent molecule coordinated to surface oxygen atoms, with one or two hydrogen atoms from EC and DMC coordinated to, respectively, one or two distinct spinel surface oxygen atoms at a distance of 1.2 Å. These particular starting configurations were motivated largely by the oxidation-induced decomposition reactions involving a highly electronegative oxygen atom (e.g. carbonyl oxygen in EC) observed in the many cluster calculations discussed above.

We found the surface reactivity to be strongly dependent on the relative electrolyte/cathode orientation, where starting configurations consisting of two hydrogen atoms from the electrolyte molecule coordinated to two different spinel surface oxygen atoms led to spontaneous proton abstraction interfacial reactions.(41) In contrast, initial electrolyte/cathode interfacial configurations with only one hydrogen atom of the electrolyte molecule coordinated to surface oxygen atoms gave a relaxed structure consisting of the electrolyte physisorbed on the NMO cathode surface. The structure relaxation calculations gave a spontaneous concerted double proton abstraction reaction for the EC/NMO[100] system and a spontaneous single proton abstraction reaction for the DMC/NMO[100] system shown in Figure 6. Similarly, a single proton is spontaneously abstracted for the reaction in the DMC/NMO[111] and EC/NMO[111] systems.(41) Our calculations agree well with recent experimental work by Kostecki et al, (58) where X-Ray absorption and fluorescence spectroscopy measurements demonstrated an electrochemical oxidation decomposition of DEC and EC on a $Li_xNi_{0.5}Mn_{1.5}O_{4-\delta}$ electrode at potentials above 4.2 V, with both stepwise and concerted proton-coupled electron transfer reactions contributing to the dissolution of transition metals.

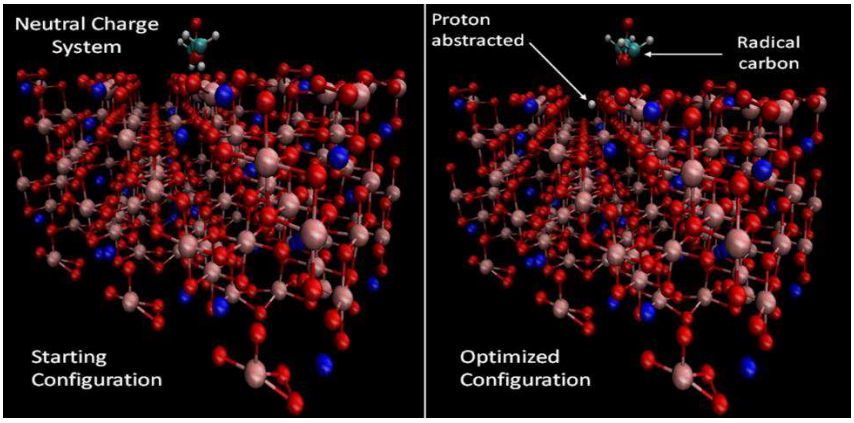

Figure 6. Initial and final configurations for geometry optimization of DMC at the NMO[100] surface from DFT calculations.

Conclusions

Screening electrolyte electrochemical stability using QC calculations has been performed for 400 isolated molecules surrounded by polarized continuum. We have found that while HOMO and LUMO energies correlate well with vertical oxidation stabilities of solvents, LUMO is not a good descriptor of the adiabatic reduction stability of many solvents due to large molecular deformation or bond breaking occurring during solvent reduction. Thus, we advocate for inclusion of the relatively expensive geometry optimization at the later stages of screening in order to obtain a more accurate prediction of the reduction stability. The second reduction potential was found to be higher than the potential for the first reduction reaction in a large number of molecules. Analogously, the second oxidation potential was found to be lower than the first oxidation potential for a significant number of solvents, indicating that if the singly oxidized radicals stick close to the cathode surface they will undergo a second oxidation.

Defluorination reactions coupled with the reduction of semifluorinated solvents in the presence of lithium were found to occur at significantly higher potentials (~ 2 V vs. Li/Li^+) compared to solvent reduction reactions that did not yield LiF during reduction (0.6-0.9 V vs. Li/Li^+ for EC/Li^+ and FEC/Li^+, respectively.) This finding is especially important because during the initial SEI formation cycle the LiF formation and deposition and radical recombination are expected to occur before the main solvent reduction reactions. Finally, the spontaneous H-abstraction reactions from carbonate solvents by cathode surface oxygens were found for the completely de-lithiated [100] and [111] surface facets of the high voltage $LiNi_{0.5}Mn_{1.5}O_4$ spinel.

References

1. K. Xu, *Chem. Rev.*, **104**, 4303 (2004).
2. K. Xu, *Chemical Reviews* (2014).
3. J. Scheers and P. Johansson, in *Electrolytes for Lithium and Lithium-Ion Batteries*, T. R. Jow, K. Xu, O. Borodin and M. Ue Editors, p. 403, Springer New York (2014).
4. M. Xu, L. Xing and W. Li, in *Electrolytes for Lithium and Lithium-Ion Batteries*, T. R. Jow, K. Xu, O. Borodin and M. Ue Editors, p. 227, Springer New York (2014).
5. K. Sodeyama, Y. Yamada, K. Aikawa, A. Yamada and Y. Tateyama, *J. Phys. Chem. C*, **118**, 14091 (2014).

6. H. Kim, F. Wu, J. T. Lee, N. Nitta, H.-T. Lin, M. Oschatz, W. I. Cho, S. Kaskel, O. Borodin and G. Yushin, *Adv. Energ. Mater.*, **5**, 1401792 (2015).
7. R. L. Wang, C. Buhrmester and J. R. Dahn, *J. Electrochem. Soc.*, **153**, A445 (2006).
8. R. L. Wang, L. M. Moshurchak, W. M. Lamanna, M. Bulinski and J. R. Dahn, *J. Electrochem. Soc.*, **155**, A66 (2008).
9. Y. K. Han, J. Jung, S. Yu and H. Lee, *J. Power Sources*, **187**, 581 (2009).
10. F. Wu, J. T. Lee, N. Nitta, H. Kim, O. Borodin and G. Yushin, *Adv. Mater.*, **27**, 101 (2015).
11. X. R. Zhang, J. K. Pugh and P. N. Ross, *J. Electrochem. Soc.*, **148**, E183 (2001).
12. M. Ue, A. Murakami and S. Nakamura, *J. Electrochem. Soc.*, **149**, A1572 (2002).
13. Y. Fu, L. Liu, H. Z. Yu, Y. M. Wang and Q. X. Guo, *J. Am. Chem. Soc.*, **127**, 7227 (2005).
14. P. Johansson, *J. Phys. Chem. A*, **111**, 1378 (2007).
15. L. D. Xing, W. S. Li, C. Y. Wang, F. L. Gu, M. Q. Xu, C. L. Tan and J. Yi, *J. Phys. Chem. B*, **113**, 16596 (2009).
16. R. S. Assary, L. A. Curtiss, P. C. Redfern, Z. C. Zhang and K. Amine, *J. Phys. Chem. C*, **115**, 12216 (2011).
17. S. P. Ong and G. Ceder, *Electrochim. Acta*, **55**, 3804 (2010).
18. N. Shao, X.-G. Sun, S. Dai and D.-e. Jiang, *J. Phys. Chem. B*, **116**, 3235 (2012).
19. N. Shao, X. G. Sun, S. Dai and D. E. Jianel, *J. Phys. Chem. B*, **115**, 12120 (2011).
20. T. Li, L. Xing, W. Li, B. Peng, M. Xu, F. Gu and S. Hu, *J. Phys. Chem. A*, **115**, 4988 (2011).
21. P. Johansson, *J. Phys. Chem. A*, **110**, 12077 (2006).
22. P. Johansson and P. Jacobsson, *J. Power Sources*, **153**, 336 (2006).
23. M. Armand and P. Johansson, *J. Power Sources*, **178**, 821 (2008).
24. J. Scheers, P. Johansson and P. Jacobsson, *J. Electrochem. Soc.*, **155**, A628 (2008).
25. L. D. Xing, C. Y. Wang, W. S. Li, M. Q. Xu, X. L. Meng and S. F. Zhao, *J. Phys. Chem. B*, **113**, 5181 (2009).
26. K. Leung, *J. Phys. Chem. C*, **116**, 9852 (2012).
27. K. Leung, Y. Qi, K. R. Zavadil, Y. S. Jung, A. C. Dillon, A. S. Cavanagh, S.-H. Lee and S. M. George, *J. Am. Chem. Soc.*, **133**, 14741 (2011).
28. J. Yu, P. B. Balbuena, J. Budzien and K. Leung, *J. Electrochem. Soc.*, **158**, A400 (2011).
29. K. Leung, *Chem Phys Lett*, **568**, 1 (2013).
30. K. Leung, S. B. Rempe, M. E. Foster, Y. Ma, J. M. Martinez del la Hoz, N. Sai and P. B. Balbuena, *J. Electrochem. Soc.*, **161**, A213 (2014).
31. P. Ganesh, P. R. C. Kent and D. E. Jiang, *J. Phys. Chem. C*, **116**, 24476 (2012).
32. K. Ushirogata, K. Sodeyama, Y. Okuno and Y. Tateyama, *J. Am. Chem. Soc.*, **135**, 11967 (2013).
33. M. M. Islam, V. S. Bryantsev and A. C. T. van Duin, *Journal of the Electrochemical Society*, **161**, E3009 (2014).
34. T. Husch, N. D. Yilmazer, A. Balducci and M. Korth, *Phys. Chem. Chem. Phys.*, **17**, 3394 (2015).
35. L. Cheng, R. S. Assary, X. Qu, A. Jain, S. P. Ong, N. N. Rajput, K. Persson and L. A. Curtiss, *J. Phys. Chem. Lett.*, 283 (2014).
36. M. Korth, *Phys. Chem. Chem. Phys.*, **16**, 7919 (2014).
37. J. S. Knap, C. E.; Borodin, O.; Leiter, K. W., *Nanotechnology* (submitted).

38. O. Borodin, W. Behl and T. R. Jow, *J. Phys. Chem. C*, **117**, 8661 (2013).
39. R. Gomer and G. Tryson, *J. Chem. Phys.*, **66**, 4413 (1977).
40. S. Trasatti, *Pure Appl Chem*, **58**, 955 (1986).
41. O. Borodin, M. Olguin, C. E. Spear, K. W. Leiter and J. Knap, *Nanotech.*, **26**, (in press) (2015).
42. M. J. T. Frisch, G. W.; Schlegel, H. B.; Scuseria, G. E.; Robb, M. A.; Cheeseman, J. R.; Scalmani, G.; Barone, V.; Mennucci, B.; Petersson, G. A.; Nakatsuji, H.; Caricato, M.; Li, X.; Hratchian, H. P.; Izmaylov, A. F.; Bloino, J.; Zheng, G.; Sonnenberg, J. L.; Hada, M.; Ehara, M.; Toyota, K.; Fukuda, R.; Hasegawa, J.; Ishida, M.; Nakajima, T.; Honda, Y.; Kitao, O.; Nakai, H.; Vreven, T.; Montgomery, J. A., Jr.; Peralta, J. E.; Ogliaro, F.; Bearpark, M.; Heyd, J. J.; Brothers, E.; Kudin, K. N.; Staroverov, V. N.; Kobayashi, R.; Normand, J.; Raghavachari, K.; Rendell, A.; Burant, J. C.; Iyengar, S. S.; Tomasi, J.; Cossi, M.; Rega, N.; Millam, N. J.; Klene, M.; Knox, J. E.; Cross, J. B.; Bakken, V.; Adamo, C.; Jaramillo, J.; Gomperts, R.; Stratmann, R. E.; Yazyev, O.; Austin, A. J.; Cammi, R.; Pomelli, C.; Ochterski, J. W.; Martin, R. L.; Morokuma, K.; Zakrzewski, V. G.; Voth, G. A.; Salvador, P.; Dannenberg, J. J.; Dapprich, S.; Daniels, A. D.; Farkas, Ö.; Foresman, J. B.; Ortiz, J. V.; Cioslowski, J.; Fox, D. J, g09, revision c, in, Gaussian, Inc., Wallingford CT, 2013 (2013).
43. Y. Zhao and D. G. Truhlar, *Theor. Chem. Acc.*, **120**, 215 (2008).
44. A. V. Marenich, C. J. Cramer and D. G. Truhlar, *J. Phys. Chem. B*, **113**, 6378 (2009).
45. O. Borodin and T. R. Jow, *ECS Transactions*, **33**, 77 (2011).
46. O. Borodin and T. R. Jow, *ECS Transactions*, **50**, 391 (2013).
47. L. Xing, O. Borodin, G. D. Smith and W. Li, *J. Phys. Chem. A*, **115**, 13896 (2011).
48. L. Xing and O. Borodin, *Phys. Chem. Chem. Phys.*, **14**, 12838 (2012).
49. Y. T. Wang, L. D. Xing, O. Borodin, W. N. Huang, M. Q. Xu, X. P. Li and W. S. Li, *Phys. Chem. Chem. Phys.*, **16**, 6560 (2014).
50. Y. Wang, L. Xing, W. Li and D. Bedrov, *J. Phys. Chem. Lett.*, **4**, 3992 (2013).
51. Z.-C. Wang, J. Xu, W.-H. Yao, Y.-W. Yao and Y. Yang, *ECS Trans.*, **41**, 29 (2012).
52. Z. Yang, A. A. Gewirth and L. Trahey, *ACS Appl. Mater, Interfaces*, **7**, 6557 (2015).
53. G. Kresse and J. Furthmuller, *Physical Review B*, **54**, 11169 (1996).
54. G. Kresse and J. Furthmuller, *Computational Materials Science*, **6**, 15 (1996).
55. G. Kresse and D. Joubert, *Physical Review B*, **59**, 1758 (1999).
56. J. Paier, M. Marsman and G. Kresse, *Journal of Chemical Physics*, **127** (2007).
57. J. P. Perdew, K. Burke and M. Ernzerhof, *Physical Review Letters*, **78**, 1396 (1997).
58. A. Jarry, S. Gottis, Y.-S. Yu, J. Roque-Rosell, C. Kim, J. Cabana, J. Kerr and R. Kostecki, *J. Am. Chem. Soc.*, **137**, 3533 (2015).